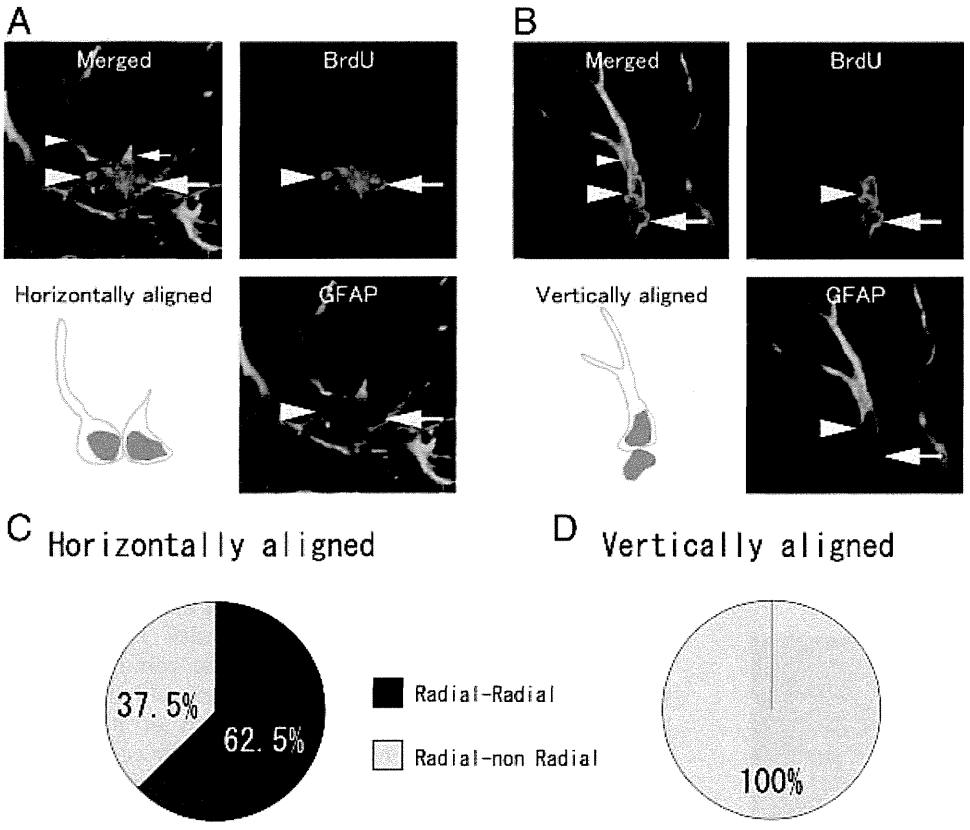

Fig. 5. Phenotype of BrdU-labeled cells in two-cell clusters in memantine-injected mice. (**A**) Example of horizontally aligned BrdU-labeled RGL progenitor cells. One RGL progenitor cell (arrowhead) possesses a long radial process (small arrowhead) and another RGL progenitor cell (arrow) has extended a short process (small arrow). Both BrdU-labeled cells (red) expressed GFAP (green). (**B**) Example of vertically aligned BrdU-labeled RGL progenitor cell (arrowhead) and non-RGL progenitor cell (arrow). The small arrowhead points to the radial process. The BrdU-labeled (red) RGL progenitor cells expressed GFAP (green), but the non-RGL progenitor cells only weakly expressed or did not express GFAP. (**C, D**) Quantitative analysis of the phenotype of BrdU-labeled cells in two-cell clusters.

clusters were formed by two RGL progenitor cells that strongly expressed GFAP (Fig. 5A,C, 62.5%, $n = 3$), suggesting a symmetric fate. In this case, one cell possessed a long radial process and another cell had a short process toward the GCL. This observation suggests that the cells had started to extend their radial processes and to become RGL cells. In contrast, almost all the vertically aligned, two-cell clusters were formed by the RGL progenitor cells and the non-RGL progenitor cells (Fig. 5B,D). The RGL progenitor cell strongly expressed GFAP, whereas the non-RGL progenitor cells weakly expressed or did not express GFAP, suggesting an asymmetric fate. No vertically aligned two-cell clusters formed by two RGL progenitor cells were observed in the present study. Taken together with the findings shown in Figs. 4 and 5, memantine probably enhances the symmetric division of RGL progenitor cells.

DISCUSSION

Neurogenesis in the hippocampus persists throughout life, and the principal source of newly generated neurons is RGL progenitor cells (primary progenitor cells) that express GFAP and/or nestin (Garcia et al., 2004; Lagace et al., 2007; Seki et al., 2007; Seri et al., 2001, 2004). Previous studies have shown that neurogenesis in the adult hippocampus is increased by NMDA-R antagonists, including MK-801 and CGP-43487 (Cameron et al., 1995; Nacher et al., 2001), but the effect of NMDA-R antagonists on RGL progenitor cells was not thoroughly investigated. In the present study, we showed that memantine, an uncompetitive NMDA-R antagonist, had increased the number of BrdU-labeled RGL progenitor cells 1 day after BrdU-injection, indicating that memantine promoted the proliferation of the RGL progenitor cells. Moreover, both the RGL morphology and the expressions of the progenitor cell markers nestin and Sox2 were sustained in the memantine-injected group for as long as 7 days after the BrdU-injection, suggesting that the properties of the progenitor cells were maintained in the newly generated cells following memantine-injection. In consequence, the number of the RGL cells in DG was increased by memantine-injection. This result is supported by the previous study, showing that a competitive NMDA-R antagonist CGP-43487 increased the number of nestin-expressing cells in the adult DG (Nacher et al., 2001). Memantine also affected the mode of cell division by the RGL progenitor cells, because the ratio of horizontally aligned RGL progenitor cells in the memantine-injected group increased significantly in comparison with that in the control group. Recent studies have shown that the alignment of daughter cells is important for determining their fate in the embryonic neocortex (Chenn and McConnell, 1995; Haydar et al., 2003), with horizontally aligned cells appearing to have a symmetric fate and vertically aligned cells appearing to have an asymmetric fate. If this is also the case in the adult hippocampus (Encinas et al., 2006; Kempermann et al., 2004), memantine appears to increase the proportion of

symmetric division in RGL progenitor cells. Taken together with the results of the present study, memantine appears to increase the population of RGL progenitor cells by promoting proliferation through the symmetric division of RGL progenitor cells. This effect of memantine on the primary progenitor cells is unique: memantine induces the expansion of the primary progenitor cell pool, because other stimulations of enhancing neurogenesis such as antidepressants, running, and enriched environment could not increase the number of the primary progenitor cells (Encinas et al., 2006; Kronenberg et al., 2003).

Despite cumulative evidence that NMDA-R antagonists promote neurogenesis, whether functional NMDA receptors are expressed in RGL progenitor cells remains controversial. Although immunohistochemical analyses in recent studies have demonstrated the expression of the NR1 and NR2B subunits of the NMDA-R in primary progenitor cells (Nacher et al., 2007), an electrophysiological study showed that the primary progenitor cells failed to respond to NMDA (Tozuka et al., 2005), indicating that the NR1 and NR2B subunits expressed in the RGL progenitor cells do not form functional NMDA-R. Consequently, it was speculated that NMDA antagonists may inhibit the neuronal activities evoked by glutamate in mature neurons and that the subsequent effects may promote the proliferation of RGL progenitor cells and neurogenesis. One potential candidate affecting the cell proliferation enhanced by memantine is FGF2, a mitogen for neural stem cells (Reynolds and Weiss, 1992). Using quantitative RT-PCR, we found that the expression of FGF2 in the GCL transiently increased by 3.7-fold on 1 day after the memantine-injection but decreased to the basal level on 2 days after the memantine-injection, whereas the expression of EGF, another major mitogen, was not affected by memantine-injection (Supp. Info. Fig. 1). These findings suggest that memantine stimulates the proliferation of RGL progenitor cells via FGF2 signaling. Further studies are needed to elucidate the mechanisms of the up-regulation of FGF2 expression by memantine-injection.

Memantine has been used clinically as a neuroprotective agent for moderate-to-severe Alzheimer's disease but has not been associated with the adverse effects, such as psychotomimetic and cardiovascular effects, shown by other NMDA-R antagonists (Johnson and Kotermanski, 2006; Reisberg et al., 2003). Jin et al. (2006) found that the administration of a clinical dose of memantine in mice (7.5 mg/kg via an intragastric route daily for 2 weeks) increased cell proliferation, and we recently confirmed that most of the newly generated cells in a group of mice injected with memantine ultimately differentiated into mature granule neurons (Maekawa et al., unpublished observations). These results suggest that the promotion of neurogenesis contributes to the therapeutic efficacy of memantine.

In conclusion, we have demonstrated that memantine significantly increases the number of RGL progenitor cells by stimulating symmetric division and that memantine enables the properties of RGL progenitor cells to be maintained in a certain number of newly generated cells, resulting in the expansion of the primary progenitor cell pool in the adult hippocampus.

ACKNOWLEDGMENT

We thank Dr. Tatsunori Seki for his kind gift of the anti-PSA-NCAM antibody.

REFERENCES

Abrous DN, Koehl M, Le Moal M. 2005. Adult neurogenesis: From precursors to network and physiology. Physiol Rev 85:523–569.

Altman J, Das GD. 1965. Autoradiographic and histological evidence of postnatal hippocampal neurogenesis in rats. J Comp Neurol 124:319–335.

Babu H, Cheung G, Kettenmann H, Palmer TD, Kempermann G. 2007. Enriched monolayer precursor cell cultures from micro-dissected adult mouse dentate gyrus yield functional granule cell-like neurons. PLoS ONE 2:e388.

Becker S, Wojtowicz JM. 2007. A model of hippocampal neurogenesis in memory and mood disorders. Trends Cognit Sci 11:70–76.

Cameron HA, McEwen BS, Gould E. 1995. Regulation of adult neurogenesis by excitatory input and NMDA receptor activation in the dentate gyrus. J Neurosci 15:4687–4692.

Chenn A, McConnell SK. 1995. Cleavage orientation and the asymmetric inheritance of Notch1 immunoreactivity in mammalian neurogenesis. Cell 82:631–641.

Doetsch F, Caille I, Lim DA, Garcia-Verdugo JM, Alvarez-Buylla A. 1999. Subventricular zone astrocytes are neural stem cells in the adult mammalian brain. Cell 97:703–716.

Encinas JM, Vaahtokari A, Enikolopov G. 2006. Fluoxetine targets early progenitor cells in the adult brain. Proc Natl Acad Sci USA 103:8233–8238.

Eriksson PS, Perfilieva E, Bjork-Eriksson T, Alborn AM, Nordborg C, Peterson DA, Gage FH. 1998. Neurogenesis in the adult human hippocampus. Nat Med 4:1313–1317.

Filippov V, Kronenberg G, Pivneva T, Reuter K, Steiner B, Wang LP, Yamaguchi M, Kettenmann H, Kempermann G. 2003. Subpopulation of nestin-expressing progenitor cells in the adult murine hippocampus shows electrophysiological and morphological characteristics of astrocytes. Mol Cell Neurosci 23:373–382.

Fukuda S, Kato F, Tozuka Y, Yamaguchi M, Miyamoto Y, Hisatsune T. 2003. Two distinct subpopulations of nestin-positive cells in adult mouse dentate gyrus. J Neurosci 23:9357–9366.

Garcia AD, Doan NB, Imura T, Bush TG, Sofroniew MV. 2004. GFAP-expressing progenitors are the principal source of constitutive neurogenesis in adult mouse forebrain. Nat Neurosci 7:1233–1241.

Haydar TF, Ang E Jr, Rakic P. 2003. Mitotic spindle rotation and mode of cell division in the developing telencephalon. Proc Natl Acad Sci USA 100:2890–2895.

Hirasawa T, Wada H, Kohsaka S, Uchino S. 2003. Inhibition of NMDA receptors induces delayed neuronal maturation and sustained proliferation of progenitor cells during neocortical development. J Neurosci Res 74:676–687.

Jin K, Xie L, Mao XO, Greenberg DA. 2006. Alzheimer's disease drugs promote neurogenesis. Brain Res 1085:183–188.

Johnson JW, Kotermanski SE. 2006. Mechanism of action of memantine. Curr Opin Pharmacol 6:61–67.

Kee N, Teixeira CM, Wang AH, Frankland PW. 2007. Preferential incorporation of adult-generated granule cells into spatial memory networks in the dentate gyrus. Nat Neurosci 10:355–362.

Kempermann G, Jessberger S, Steiner B, Kronenberg G. 2004. Milestones of neuronal development in the adult hippocampus. Trends Neurosci 27:447–452.

Kriegstein A, Noctor S, Martinez-Cerdeno V. 2006. Patterns of neural stem and progenitor cell division may underlie evolutionary cortical expansion. Nat Rev Neurosci 7:883–890.

Kronenberg G, Reuter K, Steiner B, Brandt MD, Jessberger S, Yamaguchi M, Kempermann G. 2003. Subpopulations of proliferating cells of the adult hippocampus respond differently to physiologic neurogenic stimuli. J Comp Neurol 467:455–463.

Kuhn HG, Dickinson-Anson H, Gage FH. 1996. Neurogenesis in the dentate gyrus of the adult rat: Age-related decrease of neuronal progenitor proliferation. J Neurosci 16:2027–2033.

Lagace DC, Whitman MC, Noonan MA, Ables JL, DeCarolis NA, Arguello AA, Donovan MH, Fischer SJ, Farnbauch LA, Beech RD, DiLeone RJ, Greer CA, Mandyam CD, Eisch AJ. 2007. Dynamic contribution of nestin-expressing stem cells to adult neurogenesis. J Neurosci 27:12623–12629.

Liu J, Solway K, Messing RO, Sharp FR. 1998. Increased neurogenesis in the dentate gyrus after transient global ischemia in gerbils. J Neurosci 18:7768–7778.

Maekawa M, Takashima N, Arai Y, Nomura T, Inokuchi K, Yuasa S, Osumi N. 2005. Pax6 is required for production and maintenance of progenitor cells in postnatal hippocampal neurogenesis. Genes Cells 10:1001–1014.

Nacher J, Rosell DR, Alonso-Llosa G, McEwen BS. 2001. NMDA receptor antagonist treatment induces a long-lasting increase in the number of proliferating cells, PSA-NCAM-immunoreactive granule neurons and radial glia in the adult rat dentate gyrus. Eur J Neurosci 13:512–520.

Nacher J, Varea E, Miguel Blasco-Ibanez J, Gomez-Climent MA, Castillo-Gomez E, Crespo C, Martinez-Guijarro FJ, McEwen BS. 2007. *N*-methyl-D-aspartate receptor expression during adult neurogenesis in the rat dentate gyrus. Neuroscience 144:855–864.

Nakagawa S, Kim JE, Lee R, Malberg JE, Chen J, Steffen C, Zhang YJ, Nestler EJ, Duman RS. 2002. Regulation of neurogenesis in adult mouse hippocampus by cAMP and the cAMP response element-binding protein. J Neurosci 22:3673–3682.

Namba T, Mochizuki H, Onodera M, Mizuno Y, Namiki H, Seki T. 2005. The fate of neural progenitor cells expressing astrocytic and radial glial markers in the postnatal rat dentate gyrus. Eur J Neurosci 22:1928–1941.

Namba T, Mochizuki H, Onodera M, Namiki H, Seki T. 2007. Postnatal neurogenesis in hippocampal slice cultures: Early in vitro labeling of neural precursor cells leads to efficient neuronal production. J Neurosci Res 85:1704–1712.

Parent JM, Yu TW, Leibowitz RT, Geschwind DH, Sloviter RS, Lowenstein DH. 1997. Dentate granule cell neurogenesis is increased by seizures and contributes to aberrant network reorganization in the adult rat hippocampus. J Neurosci 17:3727–3738.

Reisberg B, Doody R, Stoffler A, Schmitt F, Ferris S, Mobius HJ. 2003. Memantine in moderate-to-severe Alzheimer's disease. N Engl J Med 348:1333–1341.

Reynolds BA, Weiss S. 1992. Generation of neurons and astrocytes from isolated cells of the adult mammalian central nervous system. Science 255:1707–1710.

Schmidt-Hieber C, Jonas P, Bischofberger J. 2004. Enhanced synaptic plasticity in newly generated granule cells of the adult hippocampus. Nature 429:184–187.

Seki T, Arai Y. 1991. Expression of highly polysialylated NCAM in the neocortex and piriform cortex of the developing and the adult rat. Anat Embryol (Berl) 184:395–401.

Seki T, Arai Y. 1993. Highly polysialylated neural cell adhesion molecule (NCAM-H) is expressed by newly generated granule cells in the dentate gyrus of the adult rat. J Neurosci 13:2351–2358.

Seki T, Arai Y. 1995. Age-related production of new granule cells in the adult dentate gyrus. Neuroreport 6:2479–2482.

Seki T, Namba T, Mochizuki H, Onodera M. 2007. Clustering, migration, and neurite formation of neural precursor cells in the adult rat hippocampus. J Comp Neurol 502:275–290.

Seri B, Garcia-Verdugo JM, Collado-Morente L, McEwen BS, Alvarez-Buylla A. 2004. Cell types, lineage, and architecture of the germinal zone in the adult dentate gyrus. J Comp Neurol 478:359–378.

Seri B, Garcia-Verdugo JM, McEwen BS, Alvarez-Buylla A. 2001. Astrocytes give rise to new neurons in the adult mammalian hippocampus. J Neurosci 21:7153–7160.

Steiner B, Klempin F, Wang L, Kott M, Kettenmann H, Kempermann G. 2006. Type-2 cells as link between glial and neuronal lineage in adult hippocampal neurogenesis. Glia 54:805–814.

Tozuka Y, Fukuda S, Namba T, Seki T, Hisatsune T. 2005. GABAergic excitation promotes neuronal differentiation in adult hippocampal progenitor cells. Neuron 47:803–815.

van Praag H, Schinder AF, Christie BR, Toni N, Palmer TD, Gage FH. 2002. Functional neurogenesis in the adult hippocampus. Nature 415:1030–1034.

von Bohlen Und Halbach O. 2007. Immunohistological markers for staging neurogenesis in adult hippocampus. Cell Tissue Res 329:409–420.

Wojtowicz JM, Askew ML, Winocur G. 2008. The effects of running and of inhibiting adult neurogenesis on learning and memory in rats. Eur J Neurosci 27:1494–1502.

Glycoconj J (2013) 30:247–256
DOI 10.1007/s10719-012-9435-9

Accumulation of free Neu5Ac-containing complex-type *N*-glycans in human pancreatic cancers

Masahiko Yabu · Hiroaki Korekane · Hidenori Takahashi · Hiroaki Ohigashi · Osamu Ishikawa · Yasuhide Miyamoto

Received: 25 June 2012 / Revised: 17 July 2012 / Accepted: 18 July 2012 / Published online: 14 August 2012

Abstract We have analyzed the structures of glycosphingolipids and intracellular free glycans in human cancers. In our previous study, trace amounts of free *N*-acetylneuraminic acid (Neu5Ac)-containing complex-type *N*-glycans with a single GlcNAc at each reducing terminus (Gn1 type) was found to accumulate intracellularly in colorectal cancers, but were undetectable in most normal colorectal epithelial cells. Here, we used cancer glycomic analyses to reveal that substantial amounts of free Neu5Ac-containing complex-type *N*-glycans, almost all of which were α2,6-Neu5Ac-linked, accumulated in the pancreatic cancer cells from three out of five patients, but were undetectable in normal pancreatic cells from all five cases. These molecular species were mostly composed of five kinds of glycans having a sequence Neu5Ac-Gal-GlcNAc-Man-Man-GlcNAc and one with the following sequence Neu5Ac-Gal-GlcNAc-Man-(Man-)Man-GlcNAc. The most abundant glycan was Neu5Acα2-6Galβ1-4GlcNAcβ1-2Manα1-3Manβ1-4GlcNAc, followed by Neu5Acα2-6Galβ1-4GlcNAcβ1-2Manα1-6Manβ1-4GlcNAc. This is the first study to show unequivocal evidence for the occurrence of free Neu5Ac-linked *N*-glycans in human cancer tissues. Our findings suggest that free Neu5Ac-linked glycans may serve as a useful tumor marker.

Keywords Free oligosaccharide · *N*-glycans · Pancreatic cancer · *N*-acetylneuraminic acid

Abbreviations

Neu5Ac	*N*-acetylneuraminic acid
SGP	Sialylglycopeptide
Cer	Ceramide
GM3	Neu5Acα3Galβ4GlcCer
LST-c	Neu5Acα6Galβ4GlcNAcβ 3Galβ4GlcCer
GM1	Galβ3GalNAcβ4(Neu5Acα3) Galβ4GlcCer
LST-a	Neu5Acα3Galβ3GlcNAcβ 3Galβ4GlcCer
Disialyl Lc_4	Neu5Acα3Galβ3(Neu5Acα6) GlcNAcβ3Galβ4GlcCer
SSEA-4	Neu5Acα3Galβ3GalNAcβ3Galα 4Galβ4GlcCer
Disialyl SSEA-3	Neu5Acα3Galβ3(Neu5Acα6) GalNAcβ3Galα4Galβ4GlcCer

Introduction

Extensive studies on the oligosaccharide structures of cancers have revealed that aberrant glycosylation occurs in essentially all types of human cancers [1–4]. Altered carbohydrate determinants, including tumor associated carbohydrate antigens such as SLe^a and SLe^x have been utilized as useful tumor

Electronic supplementary material The online version of this article (doi:10.1007/s10719-012-9435-9) contains supplementary material, which is available to authorized users.

M. Yabu · Y. Miyamoto (✉)
Department of Immunology,
Osaka Medical Center for Cancer and Cardiovascular Diseases,
1-3-3 Nakamichi, Higashinari-ku,
Osaka 537-8511, Japan
e-mail: miyamoto-ya@mc.pref.osaka.jp

H. Korekane
Systems Glycobiology Research Group,
Chemical Biology Department, RIKEN Advanced Science Institute,
2-1 Hirosawa,
Wako, Saitama 351-0198, Japan

H. Takahashi · H. Ohigashi · O. Ishikawa
Department of Surgery,
Osaka Medical Center for Cancer and Cardiovascular Diseases,
1-3-3 Nakamichi, Higashinari-ku,
Osaka 537-8511, Japan

markers for the diagnosis of cancer [5–7]. Thus, the application of glycomic analyses to cancer research can highlight changes in the profiling of glycan structures during tumor development, leading to the identification of novel carbohydrate tumor markers. Hence, we comprehensively and precisely analyzed the structures of glycosphingolipids (GSLs) using highly purified colorectal cancer cells and normal colorectal epithelial cells from more than 60 patients and identified two kinds of novel tumor-associated carbohydrate antigens, Neu5Acα2-6(Fucα1-2)Galβ1-4GlcNAcβ1-3Galβ1-4Glc (α2-6-sialylated type 2H) and Neu5Acα2-6(Fucα1-2)Galβ1-3GlcNAcβ1-3Galβ1-4Glc (α2-6-sialylated type 1H), both of which are isomers of SLe^a and SLe^x [8–11]. The α2-6-sialylated type 2H was found in colorectal cancer cells from half of the cases, whilst α2-6-sialylated type 1H was specifically found in colorectal cancer cells from Lewis-negative patients. The suitability of these two carbohydrate antigens as tumor markers is currently being evaluated in our group.

In the present study, extensive structural analyses of oligosaccharides derived from pancreatic cancers have been undertaken. These analyses revealed the occurrence of substantial amounts of intracellular free Neu5Ac (*N*-acetylneuraminic acid)-containing complex-type *N*-glycans with a single GlcNAc at each reducing terminus in human pancreatic cancers. We observed both free glycans and GSLs in our assay. These molecules are extractable in chloroform-methanol solution, which was used to homogenize the cancer cells and tissues [12].

The occurrence of free high-mannose type *N*-glycans is well demonstrated in mammalian cells [13–15]. However, with the exception of mouse liver and two kinds of human stomach cancer derived cell lines (MKN7 and MKN45) [12, 16], free complex-type *N*-glycans, especially sialylated species, are not normally observed.

In our previous study, free Neu5Ac-containing complex-type *N*-glycans were found in colorectal cancers, but only at trace amounts [11]. However, a large amount of free Neu5Ac-containing complex-type *N*-glycans were found to accumulate in some pancreatic cancers. In this paper, the detailed structures of these free sialylated complex-type *N*-glycans that accumulate in human cancers are presented.

Materials and methods

The majority of the experimental procedures including purification of cancer cells and normal epithelial cells, isolation of GSLs and free oligosaccharides, preparation and separation of pyridylaminated (PA)-oligosaccharides, and mass spectrometry analyses have been reported previously [11]. In brief, pancreatic cancer cells and normal pancreatic epithelial cells were highly purified from primary lesions of pancreatic cancers and their surrounding normal pancreatic lesions, respectively, using the epithelial cell marker, CD326, and magnetic beads. CD326 positive cells were extracted with 1,200 μl of chloroform/methanol (2:1, v/v), followed by 800 μl of chloroform/methanol/water (1:2:0.8, v/v/v). This methodology extracts both GSLs and free oligosaccharides. The extracts were loaded onto a DEAE-Sephadex A25 column and flow-through fractions were collected as neutral oligosaccharides. Acidic oligosaccharides were subsequently eluted with 200 mM ammonium acetate in methanol. The neutral and acidic fractions were digested with endoglycoceramidase II from *Rhodococcus* Sp. (Takara Bio) to release the oligosaccharide portion from GSLs. Liberated oligosaccharides from GSLs and free oligosaccharides were then labeled with 2-aminopyridine (2-AP) [17].

PA-oligosaccharides were separated on a Shimadzu LC-20A HPLC system equipped with fluorescence detector. Normal phase HPLC was performed on a TSK gel Amide-80 column (0.2×25 cm, Tosoh). The molecular size of each PA-oligosaccharide is given in glucose units (Glc) based on the elution times of PA-isomaltooligosaccharides. Reversed phase HPLC was performed on a TSK gel ODS-80Ts column (0.2× 15 cm, Tosoh). The retention time of each PA-oligosaccharide is given in glucose units based on the elution times of PA-isomaltooligosaccharides. Thus, a given compound on these two columns provides a unique set of Glc (amide) and Gu (ODS) values, which correspond to coordinates of the 2-D map. PA-oligosaccharides were analyzed by LC/ESI MS/MS according to our previously established procedures [9].

Glycosidase digestions

Linkage position of Neu5Ac to the terminal galactose was determined as described previously [9]. Briefly, Neu5Ac-linked PA-oligosaccharides were digested with 2 U/ml of α2,3-sialidase from *Salmonella typhimurium* (Takara Bio) in 100 mM sodium acetate buffer, pH 5.5, for 2 h at 37 °C. Under these conditions, α2,3-sialidase specifically digests α2-3-Neu5Ac linked to the terminal residue, but not Neu5Ac with an α2-6-linkage. However, under conditions using 10 U/ml for 16 h, even so-called α2,3-sialidase can hydrolyze α2-6-Neu5Ac linked to the terminal residue, but not Neu5Ac linked to a non-terminal residue.

Preparation of free Neu5Ac-containing complex-type *N*-glycans

Authentic PA-oligosaccharides required for the analysis of GSLs have been already obtained in our laboratory and are listed in Table 1. However, we had no authentic PA-oligosaccharides of free oligosaccharides, and they were not commercially available. Hence, authentic PA-oligosaccharides of free oligosaccharides required for this study were prepared enzymatically. The procedure is outlined in Fig. 1. PA-oligosaccharides were prepared from sialylglycopeptide (SGP) (Tokyo Chemical Industry) (Fig. 1) and the results are

Table 1 Structures and elution positions in HPLC of standard PA-oligosaccharides. Peak numbers shown in Fig. 2 are given in parentheses

Abbreviation	Structure	Elution position in HPLC	
		Size (Gu)	RP (Gu)
GM3 (G1)	Neu5Acα2-3Galβ1-4Glc-PA	2.46	3.00
LST-c (G2)	Neu5Acα2-6Galβ1-4GlcNAcβ1-3Galβ1-4Glc-PA	4.40	3.76
GM1 (G3)	Galβ1-3GalNAcβ1-4Galβ1-4Glc-PA 3 | Neu5Acα2	3.85	2.92
LST-a (G4)	Neu5Acα2-3Galβ1-3GlcNAcβ1-3Galβ1-4Glc-PA	4.01	4.69
Disialyl Lc_4 (G5)	Neu5Acα2-3Galβ1-3GlcNAcβ1-3Galβ1-4Glc-PA 6 | Neu5Acα2	4.52	5.54
SSEA-4 (G6)	Neu5Acα2-3Galβ1-3GalNAcβ1-3Galα1-4Galβ1-4Glc-PA	4.98	4.81
Disialyl SSEA-3 (G7)	Neu5Acα2-3Galβ1-3GalNAcβ1-3Galα1-4Galβ1-4Glc-PA 6 | Neu5Acα2	5.26	7.47
S1-4G-Hex	Neu5Acα2-6Galβ1-4GlcNAcβ1-2Manα1 \ 6 Manβ1-4GlcNAc-PA 3 / Manα1	6.11	6.55
S2-4G-Hex (F6)	Manα1 \ 6 Manβ1-4GlcNAc-PA 3 / Neu5Acα2-6Galβ1-4GlcNAcβ1-2Manα1	6.01	5.15
S1-4G-Hex-Man (F4)	Neu5Acα2-6Galβ1-4GlcNAcβ1-2Manα1 \ 6 Manβ1-4GlcNAc-PA	5.21	5.93
S2-4G-Hex-Man (F3-2)	Manβ1-4GlcNAc-PA 3 / Neu5Acα2-6Galβ1-4GlcNAcβ1-2Manα1	5.00	6.84

summarized in Table 1. Two hundred micrograms of SGP was digested with 0.5 U/ml of recombinant endoglycosidase F2 from *Elizabethkingia meningosepticum* (Merck) in 100 mM sodium acetate buffer, pH 4.5, for 16 h at 37 °C. The released Gn1-type oligosaccharide (designated as SGP-F2, Fig. 1) was labeled with 2-aminopyridine (PA-SGP-F2). To cleave either side of the mannose arm, PA-SGP-F2 was partially digested with 1 U/ml of α2,3-sialidase from *S. typhimurium* in 100 mM sodium acetate buffer pH 5.5, for 16 h at 37 °C. Under these conditions, even so-called α2,3-sialidase can partially hydrolyze α2-6-Neu5Ac linked to the terminal residue. Two kinds of single digested oligosaccharides (S1 and S2) were separated and collected by reversed phase HPLC. S1 and S2 were sequentially digested with 0.4 U/ml β1,4-galactosidase from *Streptococcus pneumonia* (Prozyme) in 100 mM sodium citrate buffer, pH 6.0, for 2 h at 37 °C, followed by 10 U/ml of β-*N*-acetylhexosaminidase from jack bean (Seikagaku Kogyo) in 100 mM sodium citrate buffer pH 5.0, for 16 h at 37 °C (S1-4G-Hex, and S2-4G-Hex). Linkage position of the non-reducing terminal mannose of the two oligosaccharides (S1-4G-Hex and S2-4G-Hex) was determined by utilizing the specificity of jack bean α-mannosidase. S1-4G-Hex and S2-4G-Hex were digested with jack bean α-mannosidase (Seikagaku Kogyo) at either 10 U/ml or 25 U/ml in 100 mM sodium acetate buffer pH 5.0 containing 2 mM $ZnCl_2$, for 16 h at 37 °C. At the lower concentration, R-Manα1-6(Manα1-3)Manβ1-4GlcNAcβ1-4GlcNAc but not R-Manα1-3(Manα1-6)Manβ1-4GlcNAcβ1-4GlcNA is susceptible, where R is not H or Man. The substrate specificity of this enzyme was described previously [18]. Digestion with a low concentration

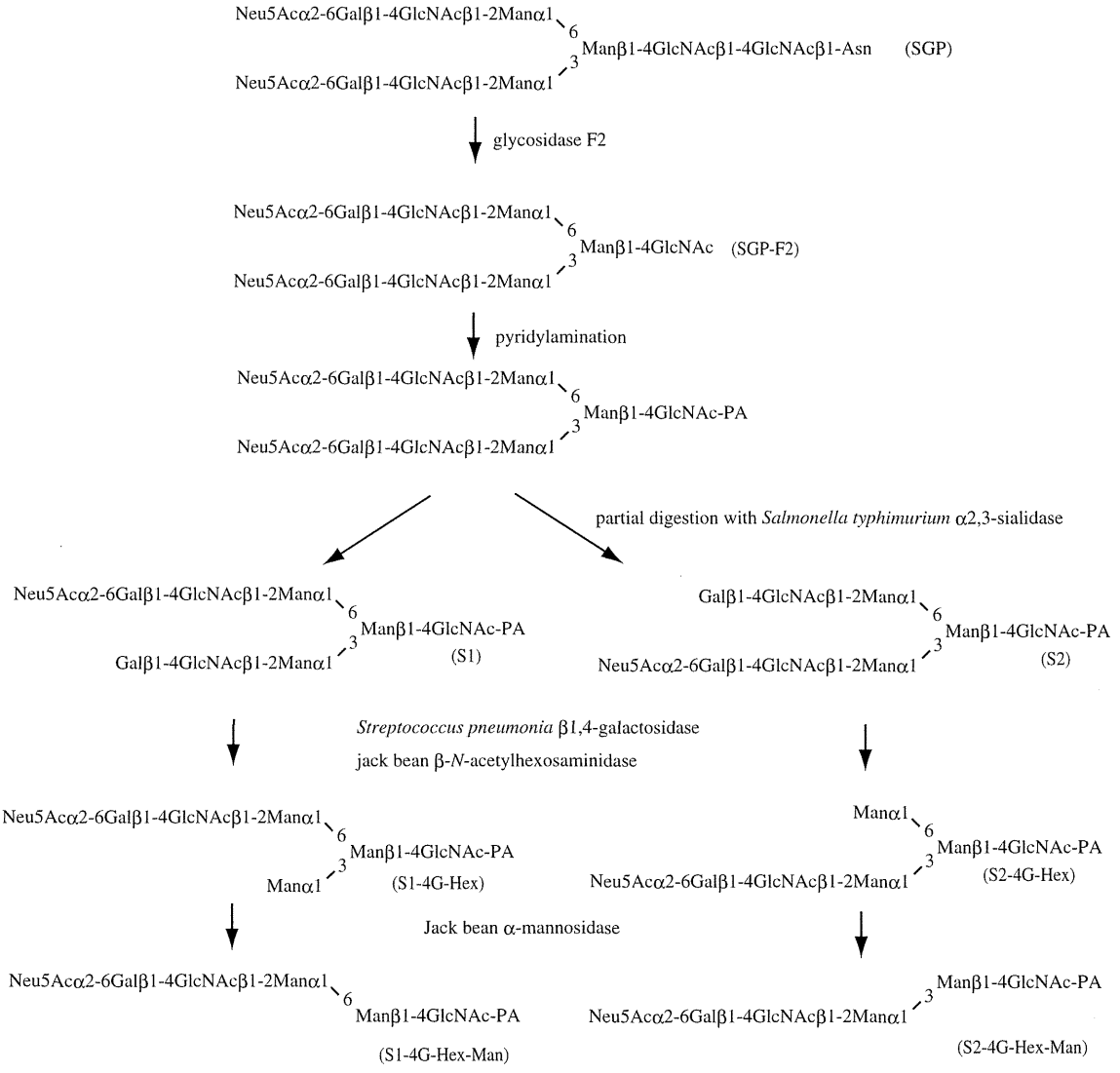

Fig. 1 The strategy used to synthesize authentic PA-free complex-type *N*-glycans

of α-mannosidase completely liberated the mannose residue from S1-4G-Hex (S1-4G-Hex-Man), indicating that the cleaved mannose was on the α1-3 side and the digested product (S1-4G-Hex-Man) was Neu5Acα2-6Galβ1-4GlcNAcβ1-2Manα1-6Manβ1-4GlcNAc-PA. S2-4G-Hex was partially cleaved by a high concentration of α-mannosidase, indicating that the cleaved mannose was on the α1-6 side and the digested product (S2-4G-Hex-Man) was Neu5Acα2-6Galβ1-4GlcNAcβ1-2Manα1-3Manβ1-4GlcNAc-PA.

Results

Preparation of PA-oligosaccharides from colon and pancreatic adenocarcinoma

Colon and pancreatic cancer cells and their normal epithelial cells were isolated with high purity from the cancer tissues and surrounding normal epithelial tissues using magnetic beads labeled with antibody against the epithelial cell marker, CD326. We analyzed the structures of GSLs and free oligosaccharides of pancreatic cancer cells and normal pancreatic cells derived from five patients. The clinicopathological features of the five pancreatic cancer patients are described in Supplementary Table 1.

It is well known that both free oligosaccharides and GSLs, but not glycoproteins, are recovered in lipid fractions from biological samples [12]. In this study, both free oligosaccharides and GSLs were extracted from the isolated cells using organic solvent, chloroform-methanol. The oligosaccharide portions of GSLs were released by endoglycoceramidase II, and the reducing ends of the released oligosaccharides of GSLs and free oligosaccharides were tagged with the fluorophore, 2-aminopyridine (see Materials and Methods).

Major acidic free oligosaccharides accumulated in human cancer cells

The acidic PA-oligosaccharides from cancer cells and normal epithelial cells were analyzed by size-fractionation HPLC (Fig. 2a–h). Each of the peaks separated by the size-fractionation HPLC was further separated by reversed phase HPLC. Additionally, the separated PA-oligosaccharides were subjected to LC/ESI MS^2 analysis. Some of the PA-oligosaccharides were also analyzed after digestion with glycosidase to help ascertain their structures. By means of these combinational analyses, the structures of all the major GSLs could be estimated and the occurrence of a large amount of free sialylated complex-type *N*-glycans in cancer cells was unequivocally demonstrated. In total, 7 distinct Neu5Ac-containing free oligosaccharides (F1, F2, F3-1, F3-2, F4, F5, and F6) were detected as major components in human pancreatic cancers (Fig. 2, Tables 2, 3). All these glycans were easily predicted to be Neu5Ac-containing free complex-type *N*-glycans having a single HexNAc (probably GlcNAc) at their reducing termini (Gn1 glycans) by mass analyses. Elution positions, mass data and estimated composition of the

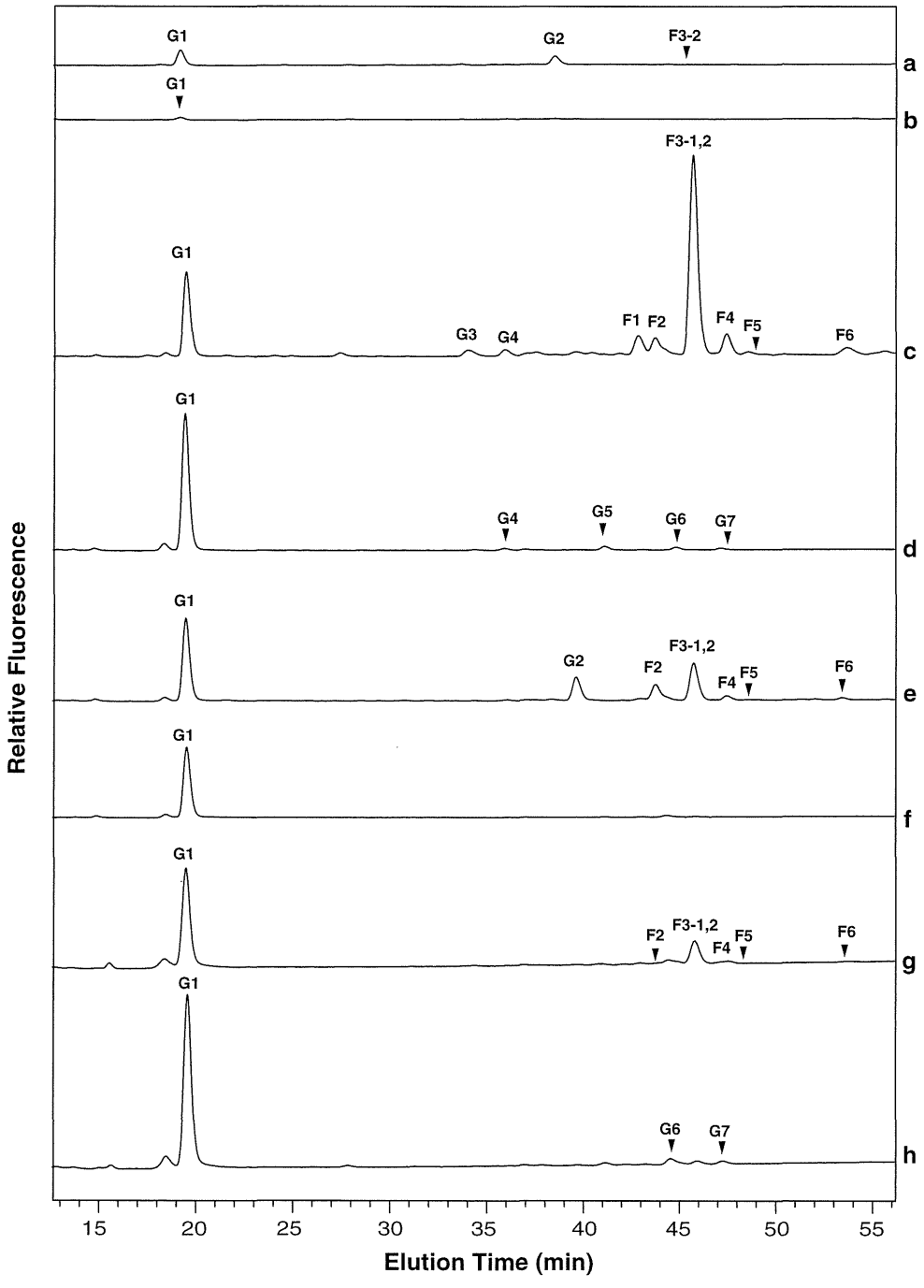

Fig. 2 Size fractionation HPLC of acidic PA-oligosaccharide mixtures obtained from human cancer and normal epithelial cells. **a** and **b** colon cancer cells (**a**) and normal colon epithelial cells (**b**) from the representative case (1×10^6 cells each), **c**–**h** pancreatic cancer cells (**c**, **e** and **g**) and normal pancreatic epithelial cells (**d**, **f** and **h**) (1×10^6 cells each). **c** and **d**, **e** and **f**, and **g** and **h** are from the same case (case 1, case 2 and case 3, respectively, Supplementary Table 1). Six major peaks derived from free *N*-glycans found in pancreatic cancer (**c**) are represented as F1–F6 with fraction numbers as per Tables 1, 2 and 3. Free *N*-glycan peaks found in other cells are numbered as per the peak numbers of C. G1–G7 are the peaks derived from GSLs. The structures of G1–G7 are listed in Table 1. The positions of minor peaks that were barely detectable are highlighted by an arrowhead

Table 2 Elution positions in HPLC and mass analysis of sialylated PA- free oligosaccharides obtained from human pancreatic cancer cells.

Group	Fraction	Elution position in HPLC		Mass (observed)	Mass (calculated)	Estimated composition
		Size (Gu)	RP (Gu)			
1	F3-1	5.03	5.55	1280.5	1280.5 $[M+H]^+$	$NeuAc_1Hex_3HexNAc_2$-PA
	F3-2	5.02	6.92	1280.4	1280.5 $[M+H]^+$	$NeuAc_1Hex_3HexNAc_2$-PA
	F4	5.26	6.00	1280.5	1280.5 $[M+H]^+$	$NeuAc_1Hex_3HexNAc_2$-PA
	F5	5.38	6.03	1280.5	1280.5 $[M+H]^+$	$NeuAc_1Hex_3HexNAc_2$-PA
	F1	4.76	7.91	1280.5	1280.5 $[M+H]^+$	$NeuAc_1Hex_3HexNAc_2$-PA
2	F6	6.07	5.20	1442.4	1442.5 $[M+H]^+$	$NeuAc_1Hex_4HexNAc_2$-PA
3	F2	4.84	7.80	1321.5	1321.5 $[M+H]^+$	$NeuAc_1Hex_2HexNAc_3$-PA

oligosaccharides are presented in Table 2. Based on the composition of monosaccharide, we were able to classify the 7 free *N*-glycans into three groups as follows; group 1 (F1, F3-1, F3-2, F4 and F5), group 2 (F6), and group 3 (F2) (Tables 2, 3). In the following results sections, the structures of these PA-oligosaccharides are explained in detail.

Structural analyses of free Neu5Ac-containing complex-type N-glycans

Group 1

The $MS^{1,2}$ spectra of the five group 1 glycans (F1, F3-1, F3-2, F4 and F5) were essentially the same. A representative $MS^{1,2}$ spectrum of F3-2 is shown in Fig. 3a, b. The structures of group 1 *N*-glycans were judged to be Neu5Ac-Hex-HexNAc-Hex-Hex-HexNAc-PA or branched Neu5Ac-HexNAc-Hex-(Hex-)Hex-HexNAc-PA by MS^2 analysis (Fig. 3a, b, Table 3), and they were anticipated to be Neu5Ac-Gal-GlcNAc-Man-Man-GlcNAc-PA or Neu5Ac-GlcNAc-Man-(Man-)Man-GlcNAc-PA, respectively. However, the latter candidate could be excluded because these oligosaccharides were resistant to jack bean α-mannosidase (data not shown). Neu5Ac is linked *via* α2-6 to the non-reducing terminal residue of F3-1, F3-2, F4 and F5, and α2-3 to that of F1 as determined by the specificity of α2-3-siallidase digestion as described in Material and Methods (Fig. 4, Table 3). These data suggested that two of the four oligosaccharides (F3-1, F3-2, F4 and F5) are

Table 3 Neu5Ac-containing free complex-type *N*-glycans accumulated in human cancers. Estimated structures and the amount of glycans in colon cancer cells (case of Fig. 2a), pancreatic cancer cells (cases of Fig. 2c, 2e, and 2g) are presented. The amount of glycan is expressed as pmol/1 × 10^6 cells. (−) indicates that this glycan was not detected in the cells

Group	Fraction	Structure	Amount of glycan (pmol/1 X 10^6 cells)			
			colon (A)	pancreas (C)	pancreas (E)	pancreas (G)
1	F3-1	Neu5Acα2-6Galβ1-4GlcNAcβ-Manα–Manβ1-4GlcNAc-PA	(-)	10.3	1.7	0.7
	F3-2	Neu5Acα2-6Galβ1-4GlcNAcβ1-2Manα1 / 3 Manβ1-4GlcNAc-PA	0.1	121.1	22.3	17.6
	F4	Neu5Acα2-6Galβ1-4GlcNAcβ1-2Manα1 \ 6 Manβ1-4GlcNAc-PA	(-)	16.6	2.9	1.9
	F5	Neu5Acα2-6Galβ1-4GlcNAcβ-Manα–Manβ1-4GlcNAc-PA	(-)	0.9	0.9	0.3
	F1	Neu5Acα2-3Galβ1-4GlcNAcβ1-2Manα1 / 3 Manβ1-4GlcNAc-PA	(-)	6.9	(-)	(-)
2	F6	Neu5Acα2-6Galβ1-4GlcNAcβ1-2Manα1 / 3 Manα1 \ 6 Manβ1-4GlcNAc-PA	(-)	2.8	1.0	0.5
3	F2	Neu5Acα2-6HexNAc-GlcNAcβ-Manα–Manβ1-4GlcNAc-PA	(-)	8.9	8.4	0.5

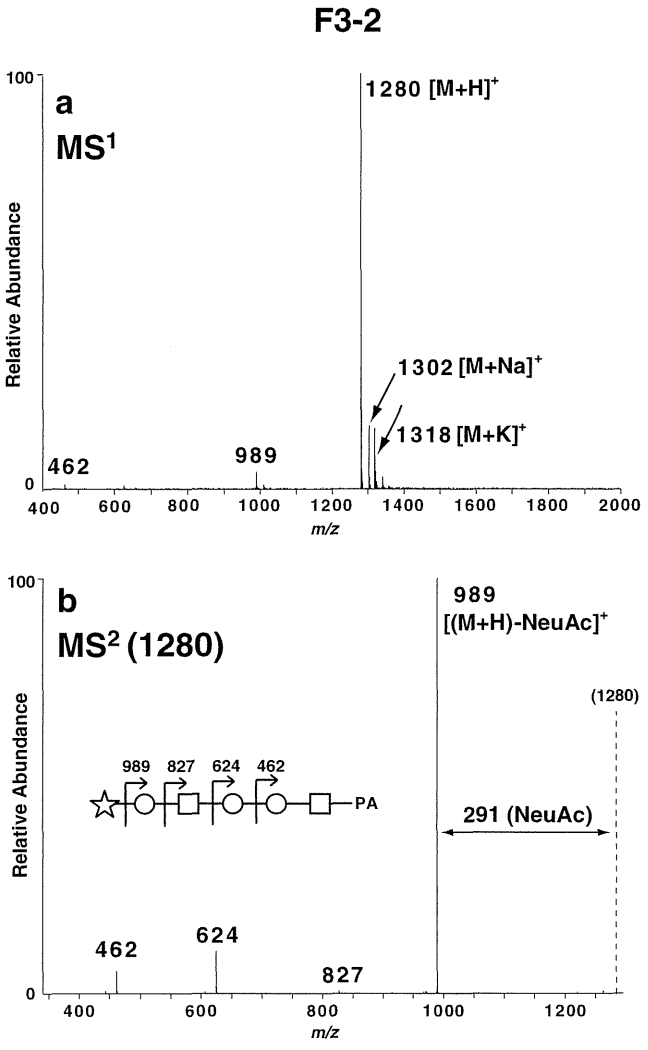

Fig. 3 $MS^{1,2}$ spectra of F3-2. **a** MS^1 spectra of F3-2; **b** MS^2 spectra of $[M+H]^+$ precursor ion at *m/z* 1280 detected in MS^1 of A. The MS/MS fragment ions were assigned as shown schematically. Symbol representations of glycans are as follows: Hex, open circle; HexNAc, open square; Neu5Ac, open star

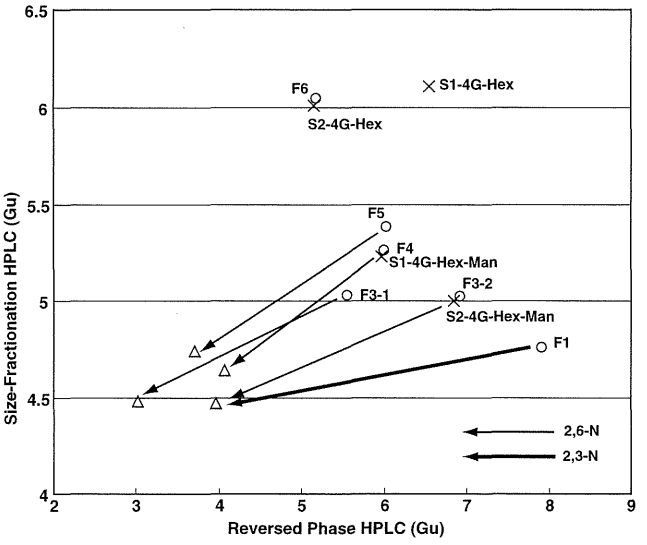

Fig. 4 Digestion of PA-oligosaccharides with sialidase. The elution profiles of PA-*N*-glycans are summarized in the form of a 2-D map. Xs indicate the positions of the authentic PA-*N*-glycans (Table 1). Open circles indicate the positions of free Neu5Ac-containing *N*-glycans, F1, F3-1, F3-2, F4, F5 and F6. Triangles indicate the positions of the digested products with sialidase. Thin lines indicate the direction of the change after α2,3-sialidase digestions of F3-1, F3-2, F4 and F5 under the conditions where the enzyme digests Neu5Ac in both α2-3- and α2-6-linkages (abbreviated as 2,6-N). Thick lines indicate the direction of the change after α2,3-sialidase digestions of F1 under the conditions where the enzyme specifically digests α2-3-linked Neu5Ac (abbreviated as 2,3-N)

likely to be digestion products of a disialylated complex biantennary *N*-glycan; specifically, cleavage of the *N,N'*-diacetylchitobiose core linkage (GlcNAcβ1-4GlcNAc) and removal of either the Manα1-3 or Manα1-6 arm from the biantennary form (Fig. 1). Hence, the authentic free complex-type *N*-glycans were synthesized from SGP (Fig. 1, see Material and Methods). F4 and F3-2 coincided with the position of the standard S1-4G-Hex-Man and S2-4G-Hex-Man, respectively, on the 2-D map (Fig. 4). These results were also confirmed by MS analyses. Thus, free oligosaccharides F4 and F3-2 were estimated to be Neu5Acα2-6Galβ1-4GlcNAcβ1-2Manα1-6Manβ1-4GlcNAc and Neu5Acα2-6Galβ1-4GlcNAcβ1-2Manα1-3Manβ1-4GlcNAc, respectively (Table 3). The structures of the other two kinds of free α2,6-Neu5Ac-linked oligosaccharides, F3-1 and F5, were thought to be either Neu5Acα2-6Galβ1-4GlcNAcβ1-6Manα1-6Manβ1-4GlcNAc or Neu5Acα2-6Galβ1-4GlcNAcβ1-4Manα1-3Manβ1-4GlcNAc, based on the branching pattern of typical tetraantennary *N*-glycans. However, we were unable to unambiguously confirm this structure. Hence, the structures of F3-1 and F5 were indicated to be Neu5Acα2-6Galβ1-4GlcNAcβ-Manα-Manβ1-4GlcNAc, without the linkage position of the fourth GlcNAc and third Man residues from the reducing terminus (Table 3). Neu5Ac is linked to F1 *via* α2-3 linkage. The desialylated product of F1 is identical to desialylated F3-2, indicating that the structure of F1 is Neu5Acα2-3Galβ1-4GlcNAcβ1-2Manα1-3Manβ1-4GlcNAc (Table 3, Fig. 4).

Group 2 and Group 3

On the 2D map, F6 coincided with the position of S2-4G-Hex, but not with S1-4G-Hex (Figs. 1 and 4). The structure of F6 was predicted to be Neu5Acα2-6Galβ1-4GlcNAcβ1-2Manα1-3(Manα1-6)Manβ1-4GlcNAc (Table 3). MS analysis revealed the compositional sequence of F2 (Group 3 glycan) to be Neu5Ac-HexNAc-HexNAc-Hex-Hex-HexNAc (data not shown). Neu5Ac was linked *via* α2-6 to the non-reducing terminus. Previous reports showed the presence of a (sialyl) LacdiNAc structure (GalNAcβ1-

4GlcNAc) [19], so we reasoned that F2 is Neu5Acα2-6GalNAc-GlcNAcβ-Manα-Manβ1-4GlcNAc. However, the subterminal residue could not be confirmed as GalNAc in this study, F2 is indicated to be Neu5Acα2-6HexNAc-GlcNAcβ-Manα-Manβ1-4GlcNAc (Table 3).

The structure of GSLs and free oligosaccharides of colorectal cancers

The profiling of acidic GSLs and free oligosaccharides of colorectal cancer cells and normal colorectal epithelial cells from representative cases are shown in Fig. 2a and b, respectively. Two major peaks, G1 (GM3) and G2 (LST-c), were obtained in acidic GSLs of colorectal cancer cells (Fig. 2a). The free oligosaccharide, corresponding to F3-2, was observed as a very minor peak, which is much lower than the GSLs, G1 (GM3) and G2 (LST-c). In the profiling of normal epithelial cells, free oligosaccharides could not be detected (Fig. 2b).

Accumulation of large amounts of free Neu5Ac-containing complex-type N-glycans in pancreatic cancer cells

The structures of GSLs and free oligosaccharides of pancreatic cancer cells and their normal pancreatic cells from five patients have been analyzed. Free oligosaccharides were obtained as major components in the pancreatic cancer cells from three out of the five cases (cases 1, 2 and 3, Supplementary Table 1). Pancreatic cancer cells derived from the two other cases contained free oligosaccharides as very minor components (cases 4 and 5, Supplementary Table 1). However, these free oligosaccharides were undetectable in normal pancreatic cells from all five cases. Furthermore, the amount of the major free *N*-glycans of pancreatic cancer cells was much higher than those of colorectal cancers cells. The profile of oligosaccharides from pancreatic cancer cells (Fig. 2c, e, g) and the corresponding normal pancreatic epithelial cells (Fig. 2d, f, h) from three cases, all of which showed an accumulation of free oligosaccharides as major components in the pancreatic cancer cells, are shown in Fig. 2c–h.

Figure 2c shows the profile of PA-glycans of case 1 (Supplementary Table 1) i.e., where free *N*-glycans were most abundantly accumulated in pancreatic cancer cells among the five cases. The corresponding profile for normal pancreatic cells from the same case is shown in Fig. 2d. In the GSLs, G1 (GM3) was expressed as the dominant component in both pancreatic cancer cells and normal pancreatic cells, and the expression levels of GM3 of these cells were much higher than those of colorectal cancer cells and normal colorectal cells (Figure 2a–d). In addition to GSLs (G1, G3 and G4), a variety of free oligosaccharides were also detected in cancer cells, but not normal cells. The abundance of the free *N*-glycans exceeded about 2-fold that of GSLs (Fig. 2c, d). Six peaks, F1, F2, F3, F4, F5 and F6, corresponding to free *N*-glycans, were observed. Reversed phase HPLC of each peak revealed that they were composed of 7 oligosaccharides, F1, F2, F3-1, F3-2, F4, F5 and F6. The abundance of each *N*-glycan is summarized in Table 3. All but 1 (F1) of the 7 glycans were α2-6-Neu5Ac-linked *N*-glycans, which represented more than 95 % of the total amount of free *N*-glycans in these samples (Table 3). F3-2 was most abundant, and the amount of other 6 glycans was much lower than that of F3-2. Among the four kinds of α2-6-sialylated oligosaccharides in group 1, the relative amount of each species was as follows: F3-2 (72 %) >>F4 (10 %)>F3-1 (6 %)>F5 (1 %) (numbers in parentheses indicate the percentage of each glycan relative to total free *N*-glycan). It is noteworthy that this order is common to all the cases of pancreatic cancers.

The profiling of GSLs and free *N*-glycans of pancreatic cancer and normal pancreatic cells from the other two cases are shown in Fig. 2e and f (case 2, Supplementary Table 1) and in Fig. 2g and h (case 3, Supplementary Table 1). The profiles are similar to that of case 1 described above, although the amounts of free *N*-glycans were considerably lower for cases 2 and 3. Nonetheless, the amount of free *N*-glycans was still comparable to that of GSLs (Fig. 2c, e, g). Akin to the previous case, the relative amount of group 1 oligosaccharides was as follows: F3-2 >>F4>F3-1>F5 (Table 3).

Discussion

Structural analyses of oligosaccharides associated with pancreatic cancers revealed, unlike colorectal cancer cells, the presence of a variety of free Neu5Ac-containing complex-type *N*-glycans. The relative amounts of these free Neu5Ac-containing complex-type *N*-glycans were comparable to or much higher than those of GSLs in most, but not all, pancreatic cancers. High levels of free Neu5Ac-containing N-glycans were observed in the pancreatic cancer cells from three out of the five cases, but correlation between clinicopathological features and the amounts of free oligosaccharides were not found.

The free *N*-glycans accumulated in cancer cells derived from the three human pancreatic cancer cases described in this study (cases 1, 2 and 3) and the previously studied colorectal cancer cases [8–11] were found to possess several common characteristic features. Specifically, (i) almost all (>95 %) of the free *N*-glycans were composed of α2-6-Neu5Ac-linked glycans, with α2-3-sialylated glycans making up a very minor part, and (ii) the proportion of each free *N*-glycan relative to total free glycans was to some extent dependent on its pentasaccharide backbone. Namely, free α2-6-

Neu5Ac-linked *N*-glycans having a Galβ1-4GlcNAcβ1-2Manα1-3Manβ1-4GlcNAc backbone were the most abundant species (i.e., 48–72 % of total free *N*-glycan content). The second most abundant glycans had a Galβ1-4GlcNAcβ1-2Manα1-6Manβ1-4GlcNAc backbone (8–24 %), followed by glycans with either a Galβ1-4GlcNAcβ1-6Manα1-6Manβ1-4GlcNAc or Galβ1-4GlcNAcβ1-4Manα1-3Manβ1-4GlcNAc backbone. These results indicated that the branch on the α6-Man arm of biantennary *N*-glycans was preferentially removed. Thus, F3-2 (Neu5Acα2-6Galβ1-4GlcNAcβ1-2Manα1-3Manβ1-4GlcNAc) was most abundant among the free Neu5Ac-containing *N*-glycans in the cancers examined.

The occurrence of free complex-type *N*-glycans in mammals has been reported in mouse liver and in human stomach cancer derived cell lines, MKN7 and MKN45 cells [12, 16]. In mouse liver, only free complex-type biantennary, but not monoantennary, *N*-glycans were observed. This observation differs from the findings reported in this study. Free monoantennary *N*-glycan was found in MKN7 and MKN45 cells. Similar to our findings, F3-2 (Neu5Acα2-6Galβ1-4GlcNAcβ1-2Manα1-3Manβ1-4GlcNAc) was most abundant in MKN7 and MKN45 cells. Furthermore, the amounts of F3-2 in MKN7 and MKN45 were about 600 and 380 pmol/10^6 cells, respectively [12]. However, significant differences in the composition of accumulated free oligosaccharides were found between the two kinds of cell lines and human pancreatic cancers. Almost all the free *N*-glycans in human cancers examined in this study were composed of monosialylated hexasaccharide with a singly trimmed core structure (group 1, and 3) along with F6 (group 2), possessing an intact trimannosyl core structure (Table 3). By contrast, in MKN7 and MKN45 cells, F3-2 was the only monosialylated hexasaccharide with a singly trimmed core structure among the various free *N*-glycans, and F6 as the major component. Furthermore, free multiply sialylated *N*-glycans, which could not be detected in human cancers, were abundantly present in MKN7 and MKN45 cells.

In the same report of MKN7 and MKN45 cells, a mechanism responsible for the accumulation of free Neu5Ac-containing *N*-glycans was suggested based on biochemical analyses to be due to insufficient lysosomal function, inefficient degradation of the free *N*-glycans in the lysosomes, as well as the leakage of lysosomal components including free *N*-glycans into the cytosol [12]. This hypothesis is further supported by the findings that F3-2, F1 and F6 are contained in excessive urinary excretion from patients with the lysosomal disease, sialidosis [20]. A similar mechanism might be responsible for the accumulation of free complex-type *N*-glycans in human pancreatic cancer cells, though experimental evidence needs to be provided by further studies.

In this study, we focused on the analysis of the structures of GSLs and fee glycans. The other kinds of glycoconjugates, such as *N*-linked glycans attached as glycoproteins, are also very interesting and important targets to investigate the difference between pancreatic and normal pancreatic cells.

In summary, we have unequivocally demonstrated that substantial amounts of free Neu5Ac-complex-type *N*-glycans accumulate in human pancreatic cancers. By contrast, in most normal epithelial cells these glycan species were undetectable. It is possible that these glycans might be developed as novel tumor markers for cancers. However, further validation studies will be needed prior to clinical application of these candidate markers.

Acknowledgements This work was supported in part by the Program for Promotion of Fundamental Studies in Health Sciences of the National Institute of Biomedical Innovation (NIBIO). This study was performed in part as a research program of the Project for Development of Innovative Research on Cancer Therapeutics (P-Direct), Ministry of Education, Culture, Sports, Science and Technology of Japan.

References

1. Hakomori, S.: Glycosylation defining cancer malignancy: new wine in an old bottle. Proc. Natl. Acad. Sci. U.S.A. **99**(16), 10231–10233 (2002)
2. Lau, K.S., Dennis, J.W.: N-Glycans in cancer progression. Glycobiology **18**(10), 750–760 (2008)
3. Brockhausen, I.: Pathways of O-glycan biosynthesis in cancer cells. Biochim. Biophys. Acta **1473**(1), 67–95 (1999)
4. Kim, Y.J., Varki, A.: Perspectives on the significance of altered glycosylation of glycoproteins in cancer. Glycoconj. J. **14**(5), 569–576 (1997)
5. Saldova, R., Wormald, M.R., Dwek, R.A., Rudd, P.M.: Glycosylation changes on serum glycoproteins in ovarian cancer may contribute to disease pathogenesis. Dis. Markers **25**(4–5), 219–232 (2008)
6. Kannagi, R., Izawa, M., Koike, T., Miyazaki, K., Kimura, N.: Carbohydrate-mediated cell adhesion in cancer metastasis and angiogenesis. Cancer Sci. **95**(5), 377–384 (2004)
7. Peracaula, R., Barrabes, S., Sarrats, A., Rudd, P.M., de Llorens, R.: Altered glycosylation in tumours focused to cancer diagnosis. Dis. Markers **25**(4–5), 207–218 (2008)
8. Shida, K., Misonou, Y., Korekane, H., Seki, Y., Noura, S., Ohue, M., Honke, K., Miyamoto, Y.: Unusual accumulation of sulfated glycosphingolipids in colon cancer cells. Glycobiology **19**(9), 1018–1033 (2009)
9. Korekane, H., Tsuji, S., Noura, S., Ohue, M., Sasaki, Y., Imaoka, S., Miyamoto, Y.: Novel fucogangliosides found in human colon adenocarcinoma tissues by means of glycomic analysis. Anal. Biochem. **364**(1), 37–50 (2007)
10. Shida, K., Korekane, H., Misonou, Y., Noura, S., Ohue, M., Takahashi, H., Ohigashi, H., Ishikawa, O., Miyamoto, Y.: Novel ganglioside found in adenocarcinoma cells of Lewis-negative patients. Glycobiology **20**(12), 1594–1606 (2010)
11. Misonou, Y., Shida, K., Korekane, H., Seki, Y., Noura, S., Ohue, M., Miyamoto, Y.: Comprehensive clinico-glycomic study of 16 colorectal cancer specimens: elucidation of aberrant glycosylation and its mechanistic causes in colorectal cancer cells. J. Proteome Res. **8**(6), 2990–3005 (2009)
12. Ishizuka, A., Hashimto, Y., Naka, R., Kinoshita, M., Kakehi, K., Seino, J., Funakoshi, Y., Suzuki, T., Kameyama, A., Narimatsu, H.: Accumulation of free complex-type N-glycans in MKN7 and MKN45 stomach cancer cells. Biochem. J. **413**(2), 227–237 (2008)

13. Moore, S.E.: Oligosaccharide transport: pumping waste from the ER into lysosomes. Trends Cell Biol. **9**(11), 441–446 (1999)
14. Suzuki, T., Funakoshi, Y.: Free N-linked oligosaccharide chains: formation and degradation. Glycoconj. J. **23**(5–6), 291–302 (2006)
15. Winchester, B.: Lysosomal metabolism of glycoproteins. Glycobiology **15**(6), 1R–15R (2005)
16. Ohashi, S., Iwai, K., Mega, T., Hase, S.: Quantitation and isomeric structure analysis of free oligosaccharides present in the cytosol fraction of mouse liver: detection of a free disialobiantennary oligosaccharide and glucosylated oligomannosides. J. Biochem. **126**(5), 852–858 (1999)
17. Natsuka, S., Hase, S.: Analysis of N- and O-glycans by pyridylamination. Methods Mol. Biol. **76**, 101–113 (1998)
18. Chen, Y.J., Wing, D.R., Guile, G.R., Dwek, R.A., Harvey, D.J., Zamze, S.: Neutral N-glycans in adult rat brain tissue–complete characterisation reveals fucosylated hybrid and complex structures. Eur. J. Biochem. **251**(3), 691–703 (1998)
19. Dell, A., Morris, H.R., Easton, R.L., Panico, M., Patankar, M., Oehniger, S., Koistinen, R., Koistinen, H., Seppala, M., Clark, G.F.: Structural analysis of the oligosaccharides derived from glycodelin, a human glycoprotein with potent immunosuppressive and contraceptive activities. J. Biol. Chem. **270**(41), 24116–24126 (1995)
20. Strecker, G., Peers, M.C., Michalski, J.C., Hondi-Assah, T., Fournet, B., Spik, G., Montreuil, J., Farriaux, J.P., Maroteaux, P., Durand, P.: Structure of nine sialyl-oligosaccharides accumulated in urine of eleven patients with three different types of sialidosis. Mucolipidosis II and two new types of mucolipidosis. Eur. J. Biochem. **75**(2), 391–403 (1977)

Published OnlineFirst on October 5, 2011; DOI:10.1158/1078-0432.CCR-11-1712

Clinical Cancer Research

Quantitative Detection of *EGFR* Mutations in Circulating Tumor DNA Derived from Lung Adenocarcinomas

Kazuya Taniguchi, Junji Uchida, Kazumi Nishino, et al.

Clin Cancer Res Published OnlineFirst October 5, 2011.

Published OnlineFirst on October 5, 2011; DOI:10.1158/1078-0432.CCR-11-1712

Clinical Cancer Research

Predictive Biomarkers and Personalized Medicine

See commentary by Lauring and Park, p. 7808

Quantitative Detection of *EGFR* Mutations in Circulating Tumor DNA Derived from Lung Adenocarcinomas

Kazuya Taniguchi[1], Junji Uchida[2], Kazumi Nishino[2], Toru Kumagai[2], Takako Okuyama[2], Jiro Okami[3], Masahiko Higashiyama[3], Ken Kodama[3], Fumio Imamura[2], and Kikuya Kato[1]

Abstract

Purpose: Examination of somatic epidermal growth factor receptor (*EGFR*) mutations is now a diagnostic routine for treatment of cancer using EGFR tyrosine kinase inhibitors (EGFR-TKI). Circulating tumor DNA is a promising target for noninvasive diagnostics. We evaluated its utility by quantitatively detecting activating and resistant mutations, which were measured with BEAMing (beads, emulsion, amplification, and magnetics).

Experimental Design: Twenty-three patients with lung cancer with progressive disease after EGFR-TKI treatment and 21 patients who had never been treated with EGFR-TKIs were studied. Their primary tumors were confirmed to have activating mutations. In the plasma DNA of each patient, the activating mutation found in the corresponding primary tumor and the T790M resistance mutation were quantified by BEAMing.

Results: In 32 of 44 patients, activating mutations were detected in the plasma DNA [72.7%; 95% confidence interval (CI), 58.0%–83.6%]. The T790M mutation was detected in 10 of 23 patients in the first group (43.5%; 95% CI, 25.6%–53.4%). The ratio of T790M to activating mutations ranged from 13.3% to 94.0%. The peak of the distribution of the mutation allele fraction in the plasma DNA was in the 0.1% to 1% range.

Conclusions: The major advantage of BEAMing is its ability to calculate the fraction of T790M-positive alleles from the alleles with activating mutations. This feature enables the detection of increases and decreases in the number of T790M mutations in cancer cells, regardless of normal cell DNA contamination, which may be useful for monitoring disease progression. Circulating tumor DNA could potentially be used as an alternative method for *EGFR* mutation detection. *Clin Cancer Res; 17(24); 1–8. ©2011 AACR.*

Introduction

The strong effects of epidermal growth factor receptor (EGFR) tyrosine kinase inhibitors (EGFR-TKI; i.e., gefitinib and erlotinib) on non–small cell lung cancer (NSCLC) are correlated with activating somatic mutations in the epidermal growth factor receptor (*EGFR*; refs. 1–3). Patients subjected to these drugs are currently selected on the basis of the presence of these activating mutations. In addition, a mutation known as T790M has been identified as a cause of gefitinib resistance (4, 5). The T790M mutation appears in about half of the cases of acquired resistance to EGFR-TKIs. Detection of T790M may have prognostic value in the patients with acquired resistance to EGFR-TKIs, because the presence of T790M defines a clinical subset with a relatively favorable prognosis and more indolent progression (6).

Detecting *EGFR* mutations using tumor tissues obtained via a biopsy or surgical resection is now routinely used to diagnose NSCLC. Because a biopsy is an invasive procedure, it is desirable to replace it with a noninvasive procedure. In particular, noninvasive tests allow the frequent monitoring of disease progression in patients with the T790M mutation (7).

For some time, circulating nucleic acids in the plasma or serum have been considered to be candidates for noninvasive cancer diagnostics (8, 9). In particular, circulating tumor DNA (ctDNA) has been explored to detect somatic mutations derived from malignant tumors. For example, in 2 studies, somatic mutations in ctDNA were used to monitor disease status with the appearance of target mutations (10, 11). One major problem is that detecting rare mutant alleles is technically difficult. Diehl and colleagues used their proprietary technique called BEAMing (beads, emulsion, amplification and magnetics; ref. 12) to measure somatic mutations in ctDNA and monitor the tumor burden during the course of the disease. In BEAMing, PCR

Authors' Affiliations: [1]Research Institute, Departments of [2]Thoracic Oncology and [3]Thoracic Surgery, Osaka Medical Center for Cancer and Cardiovascular Diseases, Higashinari-ku, Osaka, Japan

Corresponding Author: Kikuya Kato, Research Institute, Osaka Medical Center for Cancer and Cardiovascular Diseases, 1-3-3 Nakamichi, Higashinari-ku, Osaka 537-8511, Japan. Phone: 81-6-6973-1209; Fax: 81-6-6973-1209; E-mail: katou-ki@mc.pref.osaka.jp

doi: 10.1158/1078-0432.CCR-11-1712

Published OnlineFirst on October 5, 2011; DOI:10.1158/1078-0432.CCR-11-1712

Translational Relevance

For therapies using EGFR-TKIs (e.g., gefitinib and erlotinib), it is essential to determine the epidermal growth factor receptor mutation status of lung cancer lesions. Although a biopsy of the primary lesion is indispensable, noninvasive diagnostics are desirable because they allow repeated testing. In particular, it is useful to follow the disease progression by monitoring the T790M status. In contrast to other techniques, beads, emulsion, amplification, and magnetics (BEAMing) can estimate the extent to which the activating mutation alleles have been converted into resistant alleles, regardless of normal DNA contamination. This information should be more suitable for monitoring the disease status. Because BEAMing also detects activating mutations with a moderate success rate, examining the ctDNA may support a diagnosis via a biopsy. It should be noted that BEAMing and next-generation sequencers are based on the same technological principle. With this study, we can predict how next generation sequencers will detect mutations in circulating tumor DNA.

products amplified from a single molecule are fixed to a single magnetic bead using emulsion PCR. The mutation site is labeled with a fluorescent probe or primer extension, and the mutated allele is quantitatively detected by counting the fluorescently labeled beads. Simply by increasing the number of beads that are analyzed, BEAMing can be more sensitive than other PCR-based techniques (13).

In this report, we used BEAMing to detect activating and resistant *EGFR* mutations in ctDNA derived from lung cancer. The results suggest that ctDNA may complement the biopsy of primary lesions as a source of *EGFR* mutation detection. Its major advantage over other techniques is its ability to calculate the fraction of T790M-positive alleles in cancer cells, regardless of normal cell DNA contamination. In particular, this approach would enable the monitoring of disease progression during EGFR-TKI therapy via the T790M mutation.

Materials and Methods

Patient characteristics

Patients with activating *EGFR* mutations in tumor tissues were selected following a biopsy examination between June 2010 and April 2011. We recruited 23 patients with progressive disease (PD) after EGFR-TKI treatment as group 1. PD is defined as the appearance of a new lesion or a 20% increase in tumor size. The duration between the detection of PD and blood sampling for BEAMing was variable. We recruited 21 patients who had never been treated with EGFR-TKIs as group 2. In all of the patients, activating EGFR mutations were found in biopsy samples using the PNA-LNA PCR clamp method (14).

Plasma samples and DNA extraction

DNA was purified from plasma obtained from 5 mL of heparin-treated blood using Agencourt Genfind version 2 (Beckman Coulter). The DNA concentration was determined by measuring the copy number of *LINE-1* (15). It should be noted that the calibration was done using intact human genomic DNA, whereas the plasma DNA was in fragments of approximately 200 bp or less. Thus, the deduced measurement may be biased to be too low.

BEAMing

BEAMing was done as described previously (16, 17), except for the use of locked nucleic acids (LNA) as the hybridization probes for single-base substitutions. Primer and probe sequences are shown in Table 1. In the initial PCR step, the target region (~100 bp) was amplified using gene-specific primers with tag sequences. Amplification was done in a 100-μL reaction mixture containing genomic DNA obtained from 400 μL of plasma, 600 pmol of primers and 2 units of KOD -Plus- DNA polymerase (Toyobo). The product was purified with a MinElute PCR Purification Kit (Qiagen).

To prepare the magnetic beads for BEAMing, a common oligonucleotide, the sequence of which was identical to the forward primer for emulsion PCR (Table 1), was synthesized using a dual biotin group at the 5′ end and a spacer 18 polyethylene glycol between the biotin group and the terminal thymidine (Integrated DNA Technologies). One nanomole of the common oligonucleotide was attached to 100 μg of MyOne streptavidin-coated magnetic beads (Dynal), as described previously (12). The beads were finally suspended in 100 μL of TK buffer (20 mmol/L Tris-HCl, pH 8.4, 50 mmol/L KCl). To prepare the emulsifier oil, 7% ABIL WE09 (Degussa), 20% mineral oil (Sigma-Aldrich) and 73% Tegosoft DEC (Degussa) were mixed by vortexing and allowed to settle for 30 minutes.

Emulsion PCR was done as follows. A 150-μL reaction mixture consisted of 15 pg of the first aforementioned PCR product, 15 μL of 10× KOD buffer, 75 pmol of the forward primer, 12 μmol of the reverse primer and 6 μL of the magnetic beads, which were prepared as described above. Next, 0.6 mL of the emulsifier oil and 5-mm Zirconia beads were added to the 150-μL reaction mixture. A water–oil emulsion was prepared in a 2-mL Eppendorf tube using a Mixer Mill MM 300 (Qiagen) at 15 Hz for 17 seconds. The reaction mixture was divided into 50-μL aliquots and amplified using the following thermal cycling protocol: 94°C for 2 minutes; 3 cycles of 98°C for 15 seconds, 64°C for 45 seconds, and 72°C for 75 seconds; 3 cycles of 98°C for 15 seconds, 61°C for 45 seconds, and 72°C for 75 seconds; 3 cycles of 98°C for 15 seconds, 58°C for 45 seconds, and 72°C for 75 seconds; and 50 cycles of 98°C for 15 seconds, 57°C for 45 seconds, and 72°C for 75 seconds.

After thermal cycling, the reaction mixture was centrifuged to separate the oil and water. After removing the supernatant, the emulsion was degraded with 400 μL of breaking buffer (5 mmol/L Tris-HCl, pH 7.5, 1% Triton X-100, 1% SDS, 100 mmol/L NaCl, 1 mmol/L EDTA) and by

Table 1. Primer list

	Name	Sequence	Modification	Target
Primers for exon amplification from plasma DNA				
exon19	Tag119del	TCCCGCGAAATTAATACGACAAGTTAAAATTCCCGTCGCTATC		
	Tag219del	GCTGGAGCTCTGCAGCTAGACCCCCACACAGCAAAG		
exon20	Tag1T790M	TCCCGCGAAATTAATACGACGCATCTGCCTCACCTCCAC		
	Tag2T790M	GCTGGAGCTCTGCAGCTAAGCAGGTACTGGGAGCCAAT		
exon21	Tag1L858R	TCCCGCGAAATTAATACGACAGCCAGGAACGTACTGGTGA		
	Tag2L858R	GCTGGAGCTCTGCAGCTATGCCTCCTTCTGCATGGTAT		
Primers for emulsion PCR				
	Tag1 (forward)	TCCCGCGAAATTAATACGAC		
	Tag2 (reverse)	GCTGGAGCTCTGCAGCTA		
Hybridization probes for detection of beads with successful amplification				
exon19	19del_BEAM_PE_b	AGCAAAGCAGAAACTCACATC	5′ biotin	
exon20	T790M_BEAM_PE_b	CGGACATAGTCCAGGAG	5′ biotin	
exon21	L858R_BEAM_PE_b	ATGCCTCCTTCTGCATGGTAT	5′ biotin	
Hybrizationprobe for BEAMing				
exon19	19del_35_49_647	GGAGATGTTTTGATAGCG	5′ Alexa647	exon 19 E746-A750del
	19del_36_50_647	CGGAGATGTCTTGATAGC	5′ Alexa647	exon 19 E746-A750del
	19del_40_57_647	TGGCTTTCGATTCCTTGA	5′ Alexa647	exon 19 L747-S752del.P753S
	19del_AATTCC_647	TGTTGCTTCTCTTGGAATT	5′ Alexa647	exon 19 E746-L747del.IP
	19del_36_55_T_647	GCTTTCGGAACCTTGATAG	5′ Alexa647	exon 19 L747-S752del. E746V
	19del_35_53_ACT_647	GGAGAAGTTTTGATAGCG	5′ Alexa647	exon 19 K745-E749del.A750K
	19del_39_56_CAG_647	TTTCGGCTGTTCCTTGAT	5′ Alexa647	exon 19 L747-T751del.S752Q
	19del_39_48_C_647	GAGATGTTGGTTCCTTGAT	5′ Alexa647	exon 19 L747-E749del.A750P
	19del_WT_488	TGTTGCTTCTCTTAATTCC	5′ Alexa488	exon 19 wild-type control
exon20	T790M_Mut_BNA_647	atgagctgcAtgatgag	5′ Alexa647	*T790M* mutation
	T790M_WT_BNA_488	tgagctgcGtgatgag	5′ Alexa488	Wild-type control for T790M
exon21	L858R_Mut_LNA_647	gtttggccCgcccaaaat	5′ Alexa647	*L858R* mutation
	L858R_WT_LNA_488	gtttggccAgcccaaaat	5′ Alexa488	Wild-type control for L858R
	T2582A_Mut_647	cacccagcTgtttggcc	5′ Alexa647	*T2582A* mutation
	T2582A_WT_488	cacccagcAgtttggcc	5′ Alexa488	Wild-type control for T2582A

Published OnlineFirst on October 5, 2011; DOI:10.1158/1078-0432.CCR-11-1712

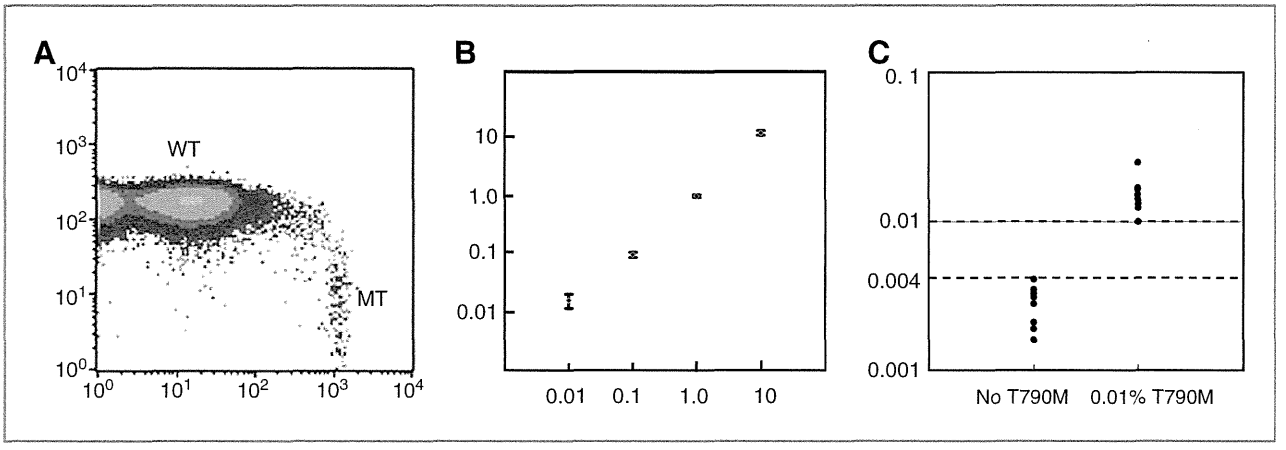

Figure 1. A, flow cytometric profile of BEAMing. The wild-type *EGFR* fragment was mixed with 0.1% of the T790M *EGFR* fragment, and BEAMing was done after PCR amplification. Horizontal axis, the fluorescence intensity of Alexa 647; vertical axis, the fluorescence intensity of Alexa 488. WT, signals from the wild-type *EGFR* fragment; MT, signals from the T789M fragment. B, linear correlation between the inoculated amount of the T790M *EGFR* fragment and the BEAMing measurement. Horizontal axis, the fraction of the T790M fragment inoculated into the wild-type fragment; vertical axis, the fraction of the T790M-positive allele measured using BEAMing. C, repeated measurements of the samples with 0.01% of the T790M fragment and those with no T790M fragment. The vertical axis indicates the fractions of the T790M-positive allele detected using BEAMing.

vortexing. After centrifugation and removal of the supernatant, the beads were washed once. Next, the DNA on the beads was denatured by 2 minutes of incubation at room temperature with 500 μL of 0.1 mol/L NaOH. After washing twice, the beads were suspended in 30 μL of distilled water.

The mutation loci were detected using allele-specific hybridization probes that consisted of locked nucleic acids and were fluorescence-labeled at their 5′ ends. Alexa 647 and Alexa 488 fluorescent dyes were used for the mutated and wild-type alleles, respectively. A hybridization probe complementary to common sequences in the mutated and wild-type alleles was manufactured via 5′ biotinylation. The hybridization reactions were carried out in a 100-μL reaction mixture consisting of 3 mol/L tetramethylammonium chloride, 50 mmol/L Tris-HCl (pH 7.5), 4 mmol/L EDTA, and 5 pmol each of the aforementioned hybridization probes. The reaction mixture was divided into 50 μL aliquots, incubated at 70°C for 10 seconds, then at 35 °C for 2 minutes after cooling down at a rate of 0.1°C/s, and additionally cooled down to room temperature using the GeneAmp PCR System 9700 Thermal Cycler (Applied Biosystems). After removing the supernatant, the beads were incubated at room temperature for 10 minutes in 20 μL of binding buffer (5 mmol/L Tris-HCl, pH 7.5, 1 mol/L NaCl, 1 mmol/L EDTA) containing 2 μg of streptavidin-conjugated phycoerythrin (PE; Invitrogen). After washing, the beads were suspended in 100 μL of TK buffer. Flow cytometric analysis was conducted with FACSCalibur (BD Bioscience) according to the manufacturer's protocol.

Results

Quantitation of the accuracy and sensitivity of BEAMing

We examined the measurement's accuracy and sensitivity using T790M as an example. We prepared normal *EGFR* gene fragments containing the mutated fragment at 10%, 1%, 0.1%, and 0.01%. These preparations were subjected to emulsion PCR. A typical example of a flow cytometric profile separating 1% T790M from the wild-type allele is shown in Fig. 1A. In BEAMing, the fractions of the mutated fragment are estimated by the ratio of the numbers of beads labeled with Alexa 647 (mutant) and those labeled with Alexa 488 (wild-type). There is a good linear correlation between the ratio deduced from the numbers of beads and the fraction of mutated fragments in the initial preparations (Fig. 1B). To determine the detection limit of BEAMing, samples without the T790M mutation and samples with 0.01% T790M mutations were analyzed repeatedly. The measurements of these 2 groups did not overlap (Fig. 1C). To confirm this result in a real experimental setting, we measured exon 19 deletion, L858R, and T790M mutations in the plasma DNA purified from 20 normal individuals. The mutation rates ranged from 0 to 0.0094 (average, 0.0021; 95% CI, 0.0012–0.0030), from 0.0009 to 0.0074 (average, 0.0025; 95% CI, 0.0019–0.0031) and from 0.0011 to 0.0097 (average, 0.0042; 95% CI 0.0030–0.0054), respectively. Thus, we set the detection limit of BEAMing as 1 in 10,000.

Activating and resistant *EGFR* mutations in plasma DNA

Plasma obtained from 44 patients was analyzed by BEAMing for the *T790M* mutation, and activating mutations were determined via a tumor biopsy. The results are shown in Table 2. In group 1, which consisted of patients who developed PD after EGFR-TKI treatment, the detection of activating and *T790M* mutations can be evaluated. In group 2, which consisted of patients who were never treated with EGFR-TKI, only those with activating mutations were evaluated. Most of the cases were in stage IV when their plasma DNA was obtained. In 32 of 44 patients, activating

Published OnlineFirst on October 5, 2011; DOI:10.1158/1078-0432.CCR-11-1712

Table 2. Allele frequency of activating and resistant *EGFR* mutations

Patient	Age, y	Sex	Histology	Stage	T790M, %	Activating mutation, %	T790M/activating mutation, %	Activating mutation type
A. Group 1 (patients with PD after EGFR-TKI treatment)								
1	56	M	adeno	4	0.029	0.058	50.8	L861Q
2	58	F	adeno	4	0.26	0.28	94.0	L858R
3	70	F	adeno	4	2.61	7.39	35.3	L858R
4	78	M	adeno	3A	0.08	0.13	65.0	L858R
5	65	M	Adeno + Sq	4	0.63	1.10	57.6	L858R
6	20	M	Adeno	4	0.14	1.03	13.3	exon 19 E746-A750del
7	41	F	adeno	4	4.28	10.3	41.6	exon 19 E746-A750del
8	59	F	adeno	4	9.54	42.7	22.3	exon 19 E746-A750del
9	53	M	adeno	4	0.16	0.19	83.6	exon 19 E746-A750del
10	49	F	adeno	4	ND	0.12	0.0	L861Q
11	75	F	adeno	4	ND	2.03	0.0	L858R
12	34	M	adeno	4	ND	0.33	0.0	L858R
13	64	M	adeno	4	ND	12.2	0.0	L858R
14	73	F	adeno	4	ND	0.046	0.0	L858R
15	66	F	adeno	4	ND	0.28	0.0	exon 19 L747-S752del.P753S
16	70	M	adeno	4	ND	11.5	0.0	exon 19 L747-S752del.P753S
17	44	F	adeno	4	ND	0.09	0.0	exon 19 L747-E749del.A750P
18	52	M	adeno	4	ND	0.74	0.0	exon 19 L747-E749del.A750P
19	74	F	adeno	4	ND	0.33	0.0	exon 19 E746-A750del
20	63	F	adeno	4	ND	ND	NA	L858R
21	65	F	adeno	4	0.10	ND	NA	exon 19 E746-A750del
22	51	F	adeno	4	ND	ND	NA	exon 19 E746-A750del
23	62	F	adeno	4	ND	ND	NA	exon 19 E746-A750del
B. Group 2 (patients not treated with EGFR-TKI)								
24	68	M	adeno	4	ND	0.17	0.0	L858R
25	45	F	adeno	4	ND	0.23	0.0	L858R
26	85	F	adeno	2B	ND	0.25	0.0	L858R
27	67	F	adeno	4	ND	0.079	0.0	L858R
28	58	F	adeno	4	ND	0.013	0.0	L858R
29	39	F	adeno	3B	ND	36.4	0.0	L858R
30	36	F	adeno	4	ND	0.11	0.0	exon 19 L747-S752del.E746V
31	56	M	adeno	4	ND	6.47	0.0	exon 19 L747-T751del.S752Q
32	55	F	adeno	3A	ND	6.24	0.0	exon 19 L747-E749del.A750P
33	65	F	adeno	3B	ND	11.8	0.0	exon 19 E746-A750del
34	76	F	adeno	4	ND	1.06	0.0	exon 19 E746-A750del
35	63	F	Sq	4	ND	0.73	0.0	exon 19 E746-A750del
36	63	M	adeno	4	ND	0.030	0.0	exon 19 E746-L747del.IP
37	72	F	adeno	4	ND	ND	NA	L858R
38	70	F	adeno	4	ND	ND	NA	L858R
39	63	M	adeno	4	ND	ND	NA	L858R
40	80	F	adeno	4	ND	ND	NA	L858R
41	70	F	adeno	4	ND	ND	NA	L858R
42	72	M	adeno	4	0.03	ND	NA	exon 19 L747-S752del.P753S
43	47	M	adeno	4	ND	ND	NA	exon 19 E746-A750del
44	54	F	adeno	4	ND	ND	NA	exon 19 E745-E749del.A750K

Abbreviations: NA, not applicable; ND, not detected.

mutations were detected in the plasma DNA (72.7%; 95% CI, 58.0–83.6%). The detection rate was higher in group 1 (group 1, 82.6%; group 2, 61.9%), but this difference was not statistically significant (the Fischer exact test, $P = 0.18$).

The detection rates of L858R/L861Q and exon 19 deletion were identical (72.7%). The T790M mutation was detected in 10 of 23 patients in group 1 (43.5%; 95% CI, 25.6%–53.4%). Because T790M accounted for about half of the

Published OnlineFirst on October 5, 2011; DOI:10.1158/1078-0432.CCR-11-1712

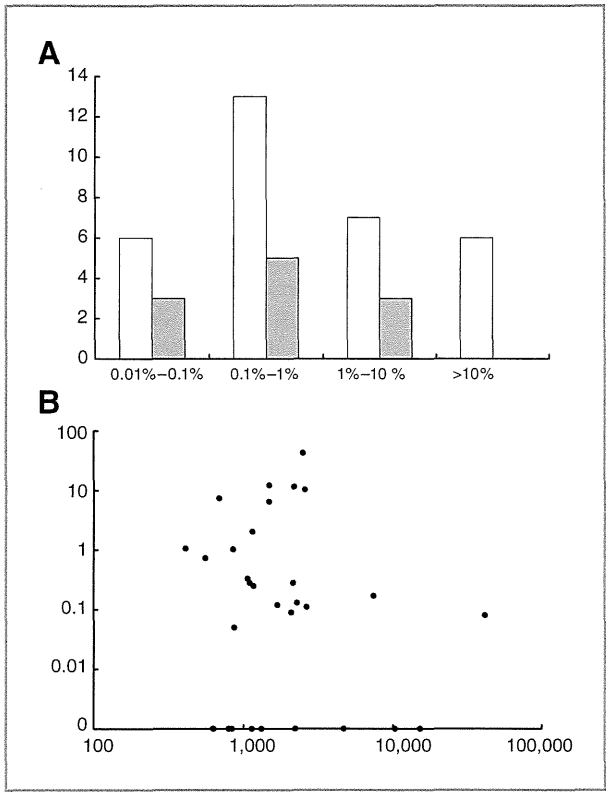

Figure 2. A, distribution of the fraction of *EGFR* molecules with activating (white columns) or resistant (gray columns) mutations in the plasma DNA. Horizontal axis, the percentage of activating EGFR mutations; vertical axis, the number of patients. B, relationship between the amount of recovered plasma DNA and the fraction of activating *EGFR* mutations. Horizontal axis, the amount of recovered plasma DNA (pg) corresponding to 400 μL of plasma; vertical axis, the percentage of activating *EGFR* mutations.

TKI-resistant cases, BEAMing was likely to detect T790M in most of the eligible cases. There were 2 cases of T790M mutations without an activating mutation (i.e., patients 21 and 42).

The fraction of ctDNA in plasma DNA can be estimated from the fraction of *EGFR* mutations [Table 2, activating mutations (%)]. On the basis of the histogram in Fig. 2A, the fraction of activating mutations varied widely across patients, and the peak of the distribution was in the 0.1% to 1% range. The fraction of the *T790M* mutation was distributed similarly but tended to shift toward lower percentages. We also investigated the relationship between the amount of recovered plasma DNA and the ctDNA deduced from the activating mutations, but we found no relationship between them (Fig. 2B). It should be noted that *EGFR* mutations were not detected in some samples with a high plasma DNA recovery.

We can deduce the number of tumor *EGFR* alleles that have been converted into resistant forms (i.e., T790M) by calculating the ratio of T790M to the number of activating mutation fractions. The ratios were within a range of 13.3% to 94.0% (Table 2), in contrast to a much wider range of tumor alleles in the plasma DNA.

Discussion

There have been a number of studies on the analysis of ctDNA to detect *EGFR* mutations in the serum or plasma DNA of NSCLC patients. These studies have mainly used techniques based on selective amplification (18, 19) or digestion (19) of specific alleles and/or high-throughput separation techniques [i.e., MALDI-TOF (20) or denaturing high performance liquid chromatography (DHPLC) (19, 21)]. The sensitivity is restricted by the specificity of the primers and enzymes in the former and by the signal-to-noise ratio in the latter. Because the sensitivity of BEAMing is only restricted by the mutations introduced during PCR (which is common to all techniques), it is theoretically more sensitive than other methods.

In addition to its high sensitivity, BEAMing allows the digital quantification of mutant alleles. The DNA in blood is derived from both tumor cells and normal cells, but we still do not know how the DNA in blood is generated. The major advantage of BEAMing is its ability to calculate the fraction of T790M-positive alleles from alleles with activating mutations. This feature enables the monitoring of the fractions of the T790M mutation in cancer cells, regardless of normal cell DNA contamination. This information should be more suitable for monitoring disease statuses. Some patients were reported to have cancer cells with T790M as a minor subpopulation before EGFR-TKI treatment (22, 23). With these cases, a qualitative assay to monitor T790M is inappropriate, and it is desirable to monitor amount of the T790M allele quantitatively. The fraction of the T790M allele would increase during the EGFR-TKI therapy and eventually reach a threshold to acquire resistance. Such threshold can be determined only with a quanititative assay. Partly due to difficulty of the biopsy of recurrent cases, clinical features of T790M-based resistance have not been fully understood, but are currently intensively studied. Such studies would find applications of the quantitative assay. For example, detecting the T790M mutation in blood samples would be useful for patient selection for treatment with new EGFR-TKIs for lung cancers that are resistant to gefitinib and erlotinib (24). One of such agents, PF00299804, is effective to a T790M-positive cell line. However, amplification of the T790M allele led to resistant to PF00299804 (25). If PF00299804 acts in patients in the same manner, quantitative monitoring of T790M allele would be useful for detection of resistance. In such patients, a biopsy of the tumor tissue is difficult and noninvasive diagnostics are highly beneficial.

The aim of this study is the initial demonstration of the technique, and has limitations as a clinical study. The patients were not enrolled in this study prospectively, and the timing of blood draws was not consistent such that the results are not directly applicable to distinct clinical situations. In addition, patients did not have serial tumor biopsies to document development of T790M in their cancer after exposure to EGFR-TKI. A well-designed prospective study enrolling more than 200 Japanese patients, a population with high incidence of activating mutation, now